

IAC-19-A3,2C,5,x52338

Lunar Navigation Beacon Network Using Global Navigation Satellite System Receivers

**Evan J. Anzalone^{a*}, Joel W. Getchius^b, Jared O. Leggett^c
Ben W. Ashman^d, Joel J. K. Parker^e, Luke B. Winternitz^f**

^a NASA/Marshall Space Flight Center, EV42, Huntsville, AL, 35801, USA, evan.j.anzalone@nasa.gov

^b NASA/Goddard Space Flight Center/Omitron, Code 595, Greenbelt, MD 20771, USA, joel.w.getchius@nasa.gov

^c NASA/Marshall Space Flight Center, EV42, Huntsville, AL, 35801, USA, jared.o.legget@nasa.gov

^d NASA/Goddard Space Flight Center, Code 595, Greenbelt, MD 20771, USA, benjamin.w.ashman@nasa.gov

^e NASA/Goddard Space Flight Center, Code 595, Greenbelt, MD 20771, USA, joel.j.k.parker@nasa.gov

^f NASA/Goddard Space Flight Center, Code 596, Greenbelt, MD 20771, USA, luke.b.winternitz@nasa.gov

* Corresponding Author

Abstract

With the increasing traffic in the lunar regime as part of NASA efforts to return humans to the moon. In order to support these missions, new capabilities are needed to support autonomous navigation and inter-asset communication. Additionally, with maturation and flight demonstration of increasingly capable small satellites, there is an opportunity to embed technology into a small spacecraft as part of companion missions. This paper addresses one such architecture, taking advantage of a lunar lander vehicle to host a companion spacecraft to build out lunar navigation and communication capability. The backbone of this spacecraft is the Navigator GPS receiver. This hardware has continually broken records on high altitude GPS coverage and has the potential to support autonomous navigation at lunar distances. This research proposes a large cubesat built around this technology and catching a ride to the moon via a lander mission. The concept of operations includes the spacecraft deploying prior to the lunar sphere of influence and maneuvering to enter into a lunar orbit. With the Navigator receiver, this spacecraft is capable of a large amount of autonomy, with a limited need for ground-based orbit determination. This spacecraft will fly alongside the lander, acting as a navigation reference during cruise, descent, and post-landing for mission validation. To assess this mission scenario, three aspects are covered in detail herein: the feasibility and mission requirements for entering into a lunar orbit given deployment along a lander surface-bound trajectory, the performance capability of the receiver along this transfer trajectory and in lunar orbit, and the ability to support navigation of the lander itself. These three areas are discussed in detail, providing results that support feasibility of the mission and determination of initial requirements.

Keywords: Navigation, GNSS, Lunar Architecture, Beacon, Planetary Lander

Acronyms/Abbreviations

GNC Ė Guidance, Navigation, and Control

GNSS Ė Global Navigation Satellite System

GPS Ė Global Positioning Systems

IMU - Inertial Measurement Unit

LPL Ė Lunar Pallet Lander

MMS - Magnetospheric Multiscale Mission

SRM Ė Solid Rocket Motor

TCM Ė Trajectory Correction Maneuver

1. Introduction

Recent priorities and investments, both government and commercial, are focusing on a return to the Lunar environment. In addition to an increase in science missions, a host of entities are developing human exploration missions. These investments lead towards a need for expanded architecture and functionality to support expansive and mature operations. In order to support numerous potential missions and maximize return, global coordination systems will be implemented to improve efficiency. To support and coordinate vehicles and explorers, a communication and navigation

network will be needed to help guide missions and provide global coverage back to Earth.

This paper focuses on the design and architecture of a proposed GNC system that utilizes advances in small-form-factor technology with special enhancements in navigation sensor hardware to provide functionality for small satellite missions in the Lunar Regime. The key technology providing navigation relative to Earth is high altitude-capable Global Positioning System (GPS) or Global Navigation Satellite System (GNSS) receivers. The proposed system specifically relies on the NASA-developed Navigator GPS receiver, which has set high altitude records, achieving GPS-derived state updates at nearly half the distance to the moon. Recent studies indicate that this technology is capable of supporting strong navigation in the Lunar domain. In the proposed system, GPS will be used to provide a high accuracy navigation and timing reference to other spacecraft.

The proposed architecture takes advantage of the GPS-based state solutions to provide navigation capability with other spacecraft through communication-based navigation approaches, allowing for inter-

spacecraft (and ground rover) state estimation. The initial use case is to support a large payload lander on approach and descent to the Lunar surface. By embedding this hardware within a small spacecraft platform, this beacon will travel from Earth alongside the lander platform. Through the use of the Navigator receiver, it is possible to provide navigation updates prior to descent.

This paper provides an overview of the capability of the navigation system in comparison to Earth-based radiometric tracking, showing reduced ground support. The LPL is simulated to show the landing accuracy enabled by the navigation beacon in orbit. These two use cases provide an overview of the potential applications and performance of the proposed network. Lastly, the paper provides a description of potential orbits for the satellite to operate in to provide services for future lunar missions.

1.1 Lander Mission Overview

This analysis uses the LPL (Lunar Pallet Lander) concept as a baseline mission scenario. The mission is defined in detail in [1, 2, 3]. The objective is to demonstrate precision landing by delivering a payload to the lunar surface within 100 meters of a landing target. Potential landing sites are selected near the lunar pole where water may be present in permanently shadowed regions that could enable future in-situ resource utilization. The LPL is part of a sequence of missions aimed at maturing the necessary technologies, such as lunar precision landing sensors that will enable the next generation of multi-ton lunar payload and human landers. An image of the vehicle is provided in Fig 1 below.

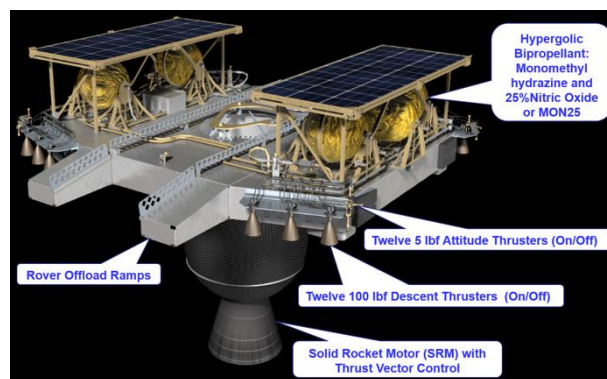


Fig. 1. Lunar Pallet Lander [2]

The LPL uses a combination of liquid propulsion and solid propulsion. The solid stage, composed of an ATK Star 48AV Solid Rocket Motor (SRM), is used for the breaking burn, and it is jettisoned after SRM burnout. The liquid propulsion consists of twelve pulsed thruster descent engines, 100 lbf each, three on each of the four corners of the vehicle, as shown in Figure 1 below. The liquid engines use a hypergolic bipropellant: a

Monomethylhydrazine (MMH) as fuel, and 25% nitric oxide (MON25) as oxidizer.

1.2 LPL Trajectory Overview

The LPL mission design assumes a ride on an Evolved Expendable Launch Vehicle (EELV) class vehicle. With the LPL as a primary payload, the mission design is greatly simplified, since the lander can fly into a direct descent to the lunar surface. Therefore, after the Trans Lunar Injection TLI burn, provided by the EELV, the LPL separates from the upper stage of the launch vehicle, as shown in the mission summary in **Error! Reference source not found.** After system checkout and sun-pointing, the LPL will perform Trajectory insertion dispersions. The mission currently budgets a total of 25 m/s of deltaV for all TCMs. After TLI, and any needed TCMs, the LPL cruises for approximately for 4 days before initiating the breaking burn with the SRM. The LPL trajectory is optimized, to account for SRM performance variations due to solid propellant temperature, **Error! Reference source not found.**, and navigation uncertainties during the SRM burn that could bias the trajectory as much as +6 km in crossrange and downrange [1, 2]. After the solid burn is completed, a short coast of 30 seconds allows the vehicle to maneuver to its optimal liquid descent burn orientation. The final liquid burn is decomposed on three phases. The first phase targets an altitude of 200 meters above the lunar surface, and a descent velocity of 10m/s [4]. Then, the second phase is a vertical descent from 200 meters down to 10 meters, with a linear ramp down in descent velocity to 1 m/s. A final descent phase is performed at a constant velocity of 1 m/s until touchdown.

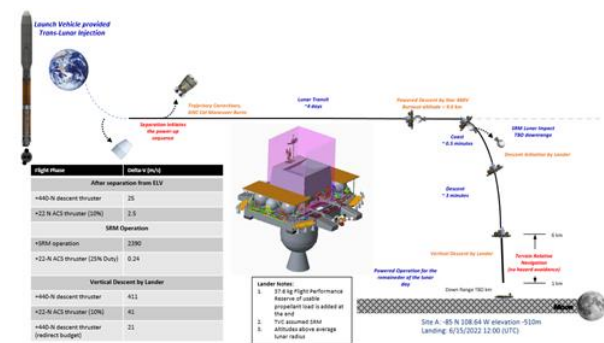


Fig 2. LPL Mission Profile [3]

2. Mission Concept of Operations

Over the next several years, a host of landers similar to LPL will be heading towards the lunar surface to demonstrate high precision and large mass capabilities. These transfers offer an opportunity to piggyback other assets and help to improve cislunar capabilities. Additionally, as more missions continue to operate in this locale, the need for in-situ capability, specifically regards

to communication and navigation will also continue to grow. One approach to address this is to place assets in orbit or on the surface via these technology and science missions to start building out the infrastructure.

2.1 Cubesat Follower Design

The fastest path to flight is to take advantage of the maturing cubesat community, with continuing expansions out into deep space, being demonstrated through the Secondary Payloads on the SLS Artemis I flight [ADD REF]. This approach has also already been successfully implemented and operated for Martian missions. Recently, NASA/JPL landed Insight on the surface of Mars. This mission included two companion spacecraft MarCO-A and MarCO-B, whose primary mission was two-fold: demonstrate the capability for cubesats to operate in deep space, and provide a communication relay for high-rate data collection during

This research assumes a similar architecture, but expands the functionality of the cubesat to include built in navigation functionality and onboard propulsion capability to enter into a lunar orbit for extended support of lunar operations, providing coverage across the moon. In order to reach the lunar environment, the cubesat is launched along with the LPL within its deployer. During cruise to the lunar sphere of influence the payload is deployed, allowing time for ground control to verify its operation, and the onboard system to get an initial fix based on the LPL state at deployment. In order to minimize onboard propellant usage, this activity is planned to happen late in the trajectory, after any trajectory corrections are performed on the lander stage.

To provide local navigation support with minimal operational support, the vehicle hosts the NASA/GSFC Navigator GPS receiver [7] which has recently achieved record high-altitude GPS observations on the Magnetospheric Multiscale Mission (MMS) spacecraft. Other studies have demonstrated the capability of this receiver to autonomously navigate using GPS at distances as far out as the moon. In order to integrate with the current version of Navigator hardware, the spacecraft will be on the larger side of cubesats, with an expected 12-24U profile. This technology is enabling force for this spacecraft, allowing it to maintain its own state (time, position, and velocity) to high accuracy. Having this knowledge onboard allows the spacecraft as a navigation beacon to provide support to other vehicles either approach cislunar space, on the surface of the planet, or traveling to/from locations in lunar regime.

2.2 Cross-link Navigation Approach

With this onboard knowledge, the spacecraft can act as a known reference point for other vehicles. This can be achieved by multiple methods. These methods can include radiometric ranging approaches such as that

described in [8, 9] where a spacecraft generates a ranging tone similar to that used in ground-based ranging. This would typically be implemented in a two-way ranging implementation where the signal is transmitted by the traveling spacecraft and retransmitted back by the reference spacecraft. Similar to ground-based operations, the receiving spacecraft can observe a change in phase of the underlying tone to measure a distance the signal has travelled. Additionally, Doppler observation of the return frequency can be used to determine how the relative change in range between the two vehicles.

An alternate approach is to embed navigation data into communications packets sent between the two spacecraft. This assumes that both spacecraft have relatively accurate onboard timing knowledge and well-calibrated software to allow for high precision time delays. Recent advancements in compact timing sources, such as the Deep Space Atomic Clock [10] and the Space Chip-Scale Atomic Clock, provide the accuracy needed for this navigation approach. This technique forms the basis of the Multi-spacecraft Autonomous Positioning System [11] that has been testing on the International Space Station in 2018 [12] and is being implemented in the form of a lunar beacon using a Space Chip-Scale Atomic Clock [13] as part of the Lunar Node É 1 payload, planning to fly in 2021 onboard a commercial lunar lander.

This study assumes a ranging capability built into the communication system of LPL with a corresponding node integrated into the follower/beacon cubesat. The analysis herein focused on the required measurement capability to focus on the performance of the proposed system with future work to study this architecture in hardware-in-the-loop analysis on flight systems.

2.3 Trajectory Design

As provided in section 1.2, LPL is assumed to be placed on a direct translunar orbit with a limited mission duration. As mentioned, this analysis assumes the follower cubesat deploys prior to the vehicle approaching the lunar Sphere of Influence to limit orbital dispersions between the two spacecraft. The baseline mission for inserting into a polar orbit is shown in Fig 3 below. This plot is shown in a lunar fixed frame, showing the approaching spacecraft and its insertion into a local orbit. Figure 4 provides more details on the evolution of the polar orbit over time. For this scenario, several orbits were considered in terms of altitude and inclination to assess coverage of the hosting lander as well as requirements on propulsion sizing. Another option considered in trajectory design was looking at lunar flyby orbits. As opposed to the spacecraft entering a fixed orbit, the constraint is to pass above the lunar surface with enough energy to fly heliocentrically and potential fullfill

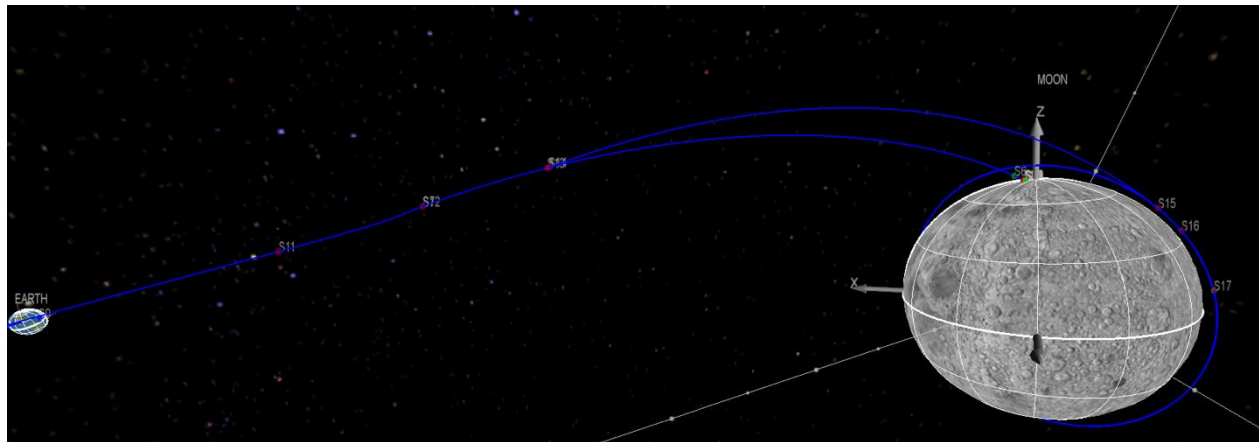


Fig. 3. Integrated trajectory showing LPL Lunar transfer and Follower insertion into polar lunar orbit

another mission, or only provide support for the descent of the spacecraft.

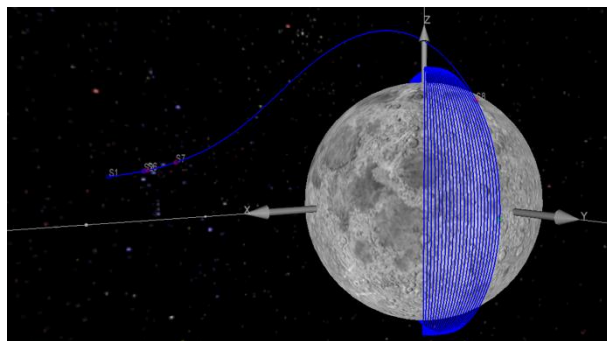


Fig. 4. Follower trajectory from deployment to orbit

4. Vehicle Sizing for Lunar Orbit Insertion

4.1 Trajectory Optimization

As proposed in this architecture, the mission will take advantage of a follower cubesat to house the Navigator receiver and provide relative navigation observations. This spacecraft will need to perform braking and transfer burns in order to remain in a defined stable lunar orbit, k] h \ ' h \ Y ' b Y WY g g U f m ' Å J ' X Y states. In order to provide insight into the design a Y W \ U b] Wg ' Z c f ' U b m ' g i W \ ' was performed using Copernicus [14]. The analysis that the CubeSat in question was on a lunar approach trajectory taken from a trajectory originally created for the LPL mission, with the reference vehicle being taken from the LPL mission 6U (assuming 1U is equivalent to 1kg) CubeSat with a specific impulse of 292.6s. For simplicity, all evaluated missions were assumed to end in a circular orbit at a lunar altitude of either 100 or 200km and at an inclination of either 0°, 45°, or 90°. This represented a broad swath of simple orbits for which a potential mission could aim.

Using Copernicus, each of the 6 evaluated missions shared a common initial segment as adapted from the

LPL mission input deck. This state was chosen to be a near entering the Lunar Sphere of Influence. The main difference between the 6 input decks was the destination orbit defined via the Keplerian elements of semi-major axis, eccentricity, and inclination as previously stated. Each mission segment inherits from the previous segment and included an optimizable impulsive burn followed by a coast for the remainder of the segment. The SNOPT algorithm was used to optimize the final solutions by minia] n] b[' h \ Y ' h c h U ' ' Å J ' f Y found that the initial design of up to 5 mission segments was insufficient for Copernicus to find viable solutions, with the first and final segments being coasting segments with variable segment times and the remainder being the braking burn for lunar capture, the burn to go from the initial lunar orbit to a potential intermediate orbit, and a final burn to put the spacecraft into the destination orbit. Empirical testing found that at least 9 segments were required, with an optimal trajectory having several small burns with magnitudes less than 1cm/s and one or two V i f b g ' Wc b g i a] b[' h \ Y ' a U ^ c f] h m ' mission. After an optimal trajectory was found for each a] g g] c b ž ' h \ Y ' h c h U ' ' Å for the U g ' f Y Wc Y j U ' i U h] c b ' c Z ' d c h Y b h] U ' ' d f c d i ' Y X ' c f V] h U

Table 1. 100 km Altitude Insertion Orbit Requirements

Inclination:	0°	45°	90°
ΔV_1 (km/s)	0.000	0.000	0.000
ΔV_2 (km/s)	0.005	0.009	0.002
ΔV_3(km/s)	0.071	0.079	0.082
ΔV_4 (km/s)	0.002	0.000	0.049
ΔV_5 (km/s)	0.000	0.000	0.002
ΔV_6 (km/s)	0.000	0.000	0.001
ΔV_7 (km/s)	0.069	0.075	0.002
ΔV_8 (km/s)	0.837	0.845	1.180
ΔV_9 (km/s)	0.000	0.000	0.000

ΔV_{Total} (km/s)	0.984	1.010	1.320
----------------------------------	--------------	--------------	--------------

Table 2. 200 km Altitude Insertion Orbit Requirements

Inclination:	0°	45°	90°
ΔV ₁ (km/s)	0.000	0.000	0.000
ΔV ₂ (km/s)	0.002	0.030	0.000
ΔV ₃ (km/s)	0.100	0.000	0.003
ΔV ₄ (km/s)	0.003	0.000	0.001
ΔV ₅ (km/s)	0.005	0.000	0.000
ΔV ₆ (km/s)	0.006	0.297	0.053
ΔV ₇ (km/s)	0.036	0.543	0.000
ΔV ₈ (km/s)	0.794	0.000	0.751
ΔV ₉ (km/s)	0.000	0.000	0.000
ΔV_{Total} (km/s)	0.946	0.870	0.809

4.2 Delta-V Requirements and Propulsion Feasibility

Once the required ΔV for each mission has been determined, it is necessary to determine any other required performance information to inform the down-selection of a propulsion system for a mission. Given the coarse state of the analysis, the required ISP for a given burn was the only independent performance parameter that could be determined. It is possible using the Tsiolkovsky equation (Eq. 1) to solve for the ratio of propellant mass to dry mass (Eq. 2), referred to as the mass ratio for the rest of this document. By constraining the mass ratio to equal 2, the minimum necessary ISP to successfully insert the vehicle into the desired lunar orbit can be calculated (see Equation 3).

$$\Delta V = I_{sp} g_0 \ln \left(\frac{m_0}{m_f} \right) \quad (1)$$

$$\frac{m_0}{m_f} = \exp \left(\frac{\Delta V}{I_{sp} g_0} \right) \quad (2)$$

$$I_{sp} = \frac{\Delta V}{g_0 \ln \left(\frac{m_0}{m_f} \right)} \quad (3)$$

From Eq. 3, the minimum acceptable ISP is directly proportionate to the natural logarithm of the mass ratio. This process informs an initial choice of a portfolio of propulsion systems that could be utilized for a given mission before a more detailed analysis can be performed.

In the previous section, the minimum required ISP for each mission was calculated using Eq. 3 and assuming that the reference gravity was 9.81 m/s². The results are shown in Table 3 and Table 4. After these minimum required ISPs had been determined, the propellant mass and mass ratios were calculated for permutations of the six

missions. The resulting distributions were used to create contour plots with the ISP ranges for various propulsion systems overlaid for clarity. Figure 5 provides insight into the propulsion sizing, showing the trend between ISP and mass fraction. Figures 6 and 7 show the total propellant mass required for a 12U and 24U platform to inform vehicle design decisions between technology readiness, mass required, and total system mass.

Table 3. ISP for 100km with Mass Fraction of 2

Inclination	0°	45°	90°
ΔV (km/s)	0.92	1.29	0.85
Min. ISP (s)	135.0	190.0	124.0

Table 4. ISP for 200km with Mass Fraction of 2

Inclination	0°	45°	90°
ΔV (km/s)	0.89	1.39	0.82
Min. ISP (s)	131.0	205.0	120.0

Optimizing the trajectories via Copernicus found that the required ΔV for each mission ranged between 0.81 and 1.32km/s in total. Using Eq. 3 to solve for the minimal ISP for each of the missions generated a range from 120 to 205s for a mass ratio of 2. Cold gas systems do not meet this required ISP performance, although all but the lowest performing hydrazine and green propulsion systems exceeded 205s. The hydrazine and green propulsion systems permit mass ratios from 2 to just less than 1.5 meaning that the propellant mass would be approximately half that of the dry mass. The remaining categories of propulsion systems (ion, pulsed plasma or vacuum arc, electrospray, and Hall Effect thrusters) enabled mass ratios of less than 1.25.

Assuming that the mass ratio must be less than 2 for any given mission, the ISP must be at least 205s for any mission analyzed herein. Based on the information found in Table 4-1 of [15], this means that all evaluated categories of propulsion systems except those using cold gas are viable options for lunar missions given the range of ΔV required. A propulsion system with an ISP exceeding 700s would permit a mass ratio of less than 1.3km/s. These rough findings should enable further, more detailed analyses on the performance of specific propulsion systems, such as a study with the modeling of finite burns instead of impulsive maneuvers for a given mission.

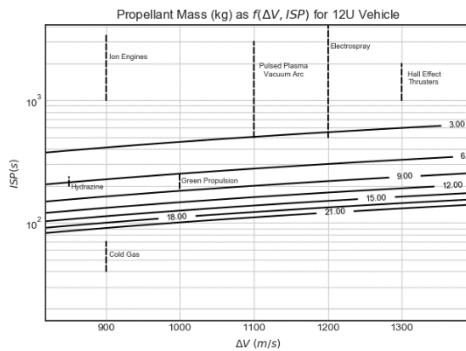
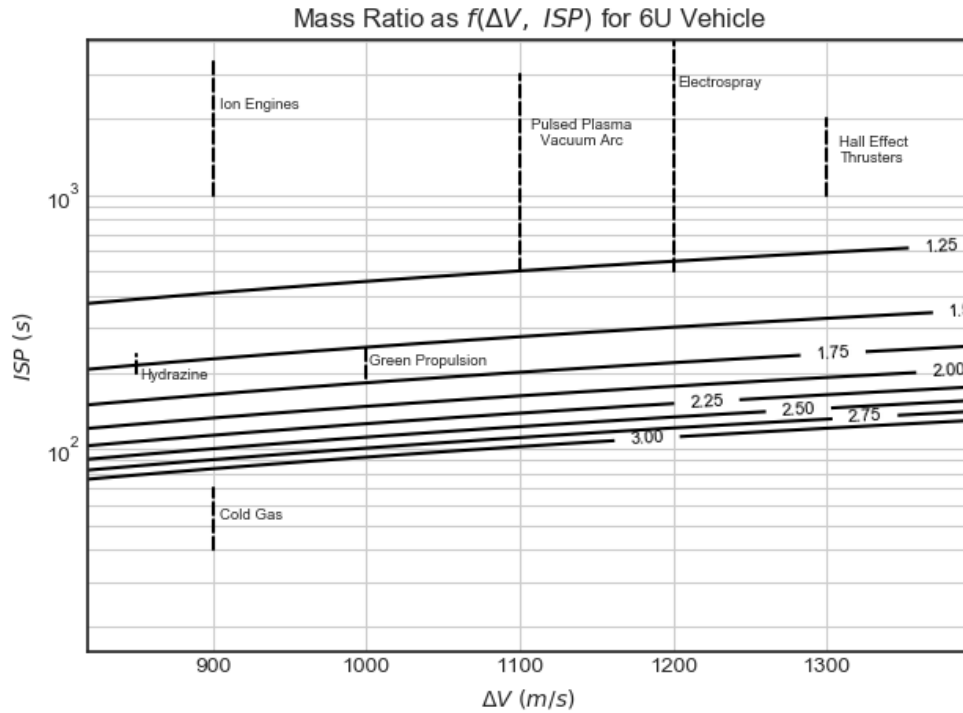


Fig. 6" 7 c b h c i f g c Z D f c d Y U b h A U d p d U d U b W h I c b C Z A J and ISP of 12U Vehicle.

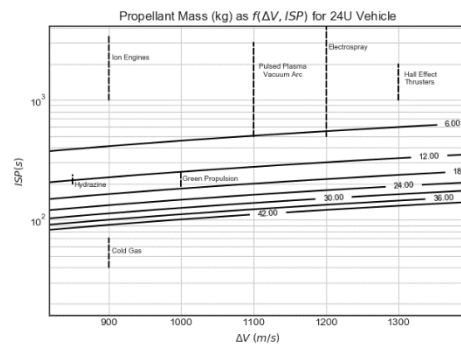


Fig. 7" 7 c b h c i f g c Z D f c d Y U b h A U d p d U d U b W h I c b C Z A J and ISP of 24U Vehicle.

5. Performance of Navigator in Representative Orbits

Given the trajectory design of the LPL and feasibility of the follower cubesat, analysis was performed using the Goddard Enhanced Orbital Navigation System (GEONS) software [16] to understand its capability. The focus of this section is to provide insight to the navigation capability using the Navigator receiver along the mission profile. Weak signal GPS and accelerometer-like performance of maneuver knowledge are the only sensors examined in this study. The weak signal GPS performance is based on the observed Magnetospheric Multiscale Mission satellite GPS hardware performance while the accelerometer performance is modelled loosely off of Orion IMU specifications (error in impulsive DV of 0.15% of maneuver). GPS measurements (L1 pseudorange) were assumed to be available every 30 seconds.

The GPS signal simulation model is based on a model of the MMS-Navigator GPS receiver augmented with a ~0.5 m diameter 14 dBi high-gain antenna, and realistic GPS link model calibrated for consistency with the on-orbit MMS GPS signal strengths. This model uses the recently released in-orbit measured per-block mean transmit patterns from the GPS Antenna Characterization Experiment (ACE) project [17] and a GPS yaw model to accurately reproduce C/N0 and visibility due to GPS transmitter sidelobes which can be the majority of visible signals in high altitude applications. The GPS simulation setup is as in [7], where further detail can be found.

$$C/N_0 = P_T + G_T \text{ fl } \checkmark \cdot \text{ l } \cdot \text{ Li} \& \$ \cdot \text{ c } (4) \text{ fl } ($$

Table 5. Calibrated Link Parameters from analysis of MMS-Navigator GPS and high-altitude MMS flight data

Link Parameter	Value
Antenna Temperature T_a	34 K
System Temperature T_{sys}	132 K
Implementation Loss R_{loss}	1.7 dB
Polarization Loss L_{pol}	1 dB
Block II/IIA P_T	17.9 dBW
(max EIRP)	(31.6 dBW)
Block IIR P_T	17.3 dBW
(max EIRP)	(29.2 dBW)
Block IIRM P_T	18.8 dBW
(max EIRP)	(32.1 dBW)
Block IIF P_T	16.2 dBW
(max EIRP)	(29.5 dBW)

A maximum of 12 GPS pseudorange (PR) measurements are simulated every 10 s with a simple unbiased additive random error model of 10 m below, and 4 m above, a 40 dB- σ noise floor. The simulated PRs, but are not in these studies. A 32 GPS SV constellation is modelled using a broadcast ephemeris file from 2017, but advanced to the current date. GPS visibility is assessed based on the GPS link model given in (4) above, Earth and Moon occultations, and a tracking performance with a sensitivity of 23 dB-Hz.

Atomic Frequency Standard (RAFS) clock [citation to datasheet] is one example of a commercially available space qualified atomic clock---which was also used in [7]. The filter was configured to solve for the position, velocity, time bias, time bias rate, and time bias acceleration. The process noise model utilized is $1e-14$ (m^2/s^2) is in line with previous studies on Gateway and MMS navigation.

The first trajectory segment studied is a lunar transfer trajectory from Low Earth Orbit to the lunar environment. Figures 8 and 9 show the position and velocity errors from a single simulation run, respectively, each separated into range and lateral components. In both position and velocity the range errors are dominant due to challenges in separating range and clock errors using GPS pseudoranges at high-altitude, without significant dynamics. Further discussion of this phenomenon is provided in reference [7]. Nonetheless, position errors remain below 60 m and velocity errors under 0.5 mm/s each channel.

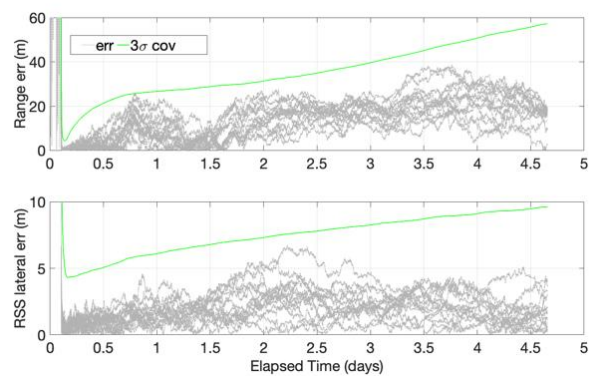


Figure 10 consists of two vertically stacked plots showing error metrics over a 5-day period. The x-axis for both plots is 'Elapsed Time (days)', ranging from 0 to 5. The top plot shows 'Range err (m/s)' on the y-axis, with a scale factor of $\times 10^{-4}$. It displays a dense cloud of grey lines representing individual realizations and a single green line representing the 3σ covariance bound. The bottom plot shows 'RS lateral err (m/s)' on the y-axis, with a scale factor of $\times 10^{-5}$. It also displays a dense cloud of grey lines and a single green line representing the 3σ covariance bound. A legend in the top plot indicates 'err = 3σ cov'.

Figures 8 and 9 show an initial convergence period followed by gradual error growth with time and distance from Earth. This is consistent with expectations; as the

uncertainty was treated as an independent error on the range observation. The covariance data was used to generate an error in each axis at the time of observation. The total offset of the computed range error was then added to the measured value as an additional error. The same trade study was completed as for the previous case and the results are in the Figure 25.

Fig. 25. Effect of Vehicle Knowledge Effects on Ground Determination Accuracy

As shown in the plot above, the knowledge of the Z c ` ` c k Y f ` ` g d U W Y W f U Z h Ð g ` ` d c knowledge of less than 100 meters. With improvements in integration of onboard accelerometer and attitude information, this capability to will continue to be refined. As shown it the analysis, this baseline performance can be used to both support high precision landing verification, as well as potential support of incoming or outgoing vehicles. The analysis presented herein focuses on the transfer during cruise and post-landing legs. The ability of integration of external measurement during planetary descent and ascent is under further study. With this capability for autonomous navigation, lunar vehicles can be designed to accomplish more complicated missions and be able to operate with minimal control from Earth-based mission control. This is increasingly important for the large number of planned lunar missions as part of the Artemis efforts.

6.4 Continued Operations

With the spacecraft in lunar orbit, it can continue to support operations in the local environment for a variety of other mission scenarios. In addition to providing coverage for surface operations in terms of navigation and communication, it can also support elements

ascending from the lunar surface and assist in state determination prior to launch. Similarly, as shown here, the vehicle can act as a beacon to support other incoming spacecraft as well as vehicles traveling between various lunar orbits.

7. Conclusions and Discussion

This research lays out a powerful architecture for enabling a breadth of navigation and communication potential for lunar-focused missions. The integration of the Navigator GPS Receiver onto a lunar cubesat provides a highly accurate timing and navigation reference source for other assets in the region. The mission herein focused on the application of a follower spacecraft flying with a lunar lander. This application exhibited great benefit to both cruise and post-landing phases of flight. This is achieved through helping to maintain an accurate onboard state at high frequency throughout flight, minimizing the need for external ground-based tracking. With this architecture, the lander able to maintain an accurate state up until lunar descent, enabling a high precision landing approach, reducing initial errors.

Furthermore, this analysis has demonstrated the expected capability of the Navigator receiver both during its transfer to the moon and while in lunar orbit. While in lunar orbit, the spacecraft was able to maintain position knowledge of less than 100 meters. With improvements in integration of onboard accelerometer and attitude information, this capability to will continue to be refined. As shown it the analysis, this baseline performance can be used to both support high precision landing verification, as well as potential support of incoming or outgoing vehicles. The analysis presented herein focuses on the transfer during cruise and post-landing legs. The ability of integration of external measurement during planetary descent and ascent is under further study. With this capability for autonomous navigation, lunar vehicles can be designed to accomplish more complicated missions and be able to operate with minimal control from Earth-based mission control. This is increasingly important for the large number of planned lunar missions as part of the Artemis efforts.

Acknowledgements

The authors would like to acknowledge the work and support of the LPL/VIPER analysis and Navigator teams at GSFC and MSFC. Their work and design form the basis of this analysis informed the scope and application of this work. Additionally, the authors would like to thank their management in support of enabling this work and documentation.

References

